



High NV density in a pink CVD diamond grown with N₂O addition

Alexandre Tallaire, Ovidiu Brinza, Paul Huillery, Tom Delord, Clément Pellet-Mary, Robert Staacke, Bernd Abel, Sébastien Pezzagna, Jan Meijer, Nadia Touati, et al.

► To cite this version:

Alexandre Tallaire, Ovidiu Brinza, Paul Huillery, Tom Delord, Clément Pellet-Mary, et al.. High NV density in a pink CVD diamond grown with N₂O addition. Carbon, 2020, 170, pp.421-429. 10.1016/j.carbon.2020.08.048 . hal-03449975

HAL Id: hal-03449975

<https://hal.science/hal-03449975>

Submitted on 6 Dec 2021

HAL is a multi-disciplinary open access archive for the deposit and dissemination of scientific research documents, whether they are published or not. The documents may come from teaching and research institutions in France or abroad, or from public or private research centers.

L'archive ouverte pluridisciplinaire **HAL**, est destinée au dépôt et à la diffusion de documents scientifiques de niveau recherche, publiés ou non, émanant des établissements d'enseignement et de recherche français ou étrangers, des laboratoires publics ou privés.

High NV density in a pink CVD diamond grown with N₂O addition

Alexandre Tallaire^{1,2*}, Ovidiu Brinza², Paul Huillery³, Tom Delord³, Clément Pellet-Mary³, Robert Staacke⁴, Bernd Abel⁴, Sébastien Pezzagna⁴, Jan Meijer⁴, Nadia Touati¹, Laurent Binet¹, Alban Ferrier¹, Philippe Goldner¹, Gabriel Hetet³, Jocelyn Achard^{2†}

¹ *IRCP, Chimie ParisTech, CNRS, PSL Research University, 11 rue Pierre et Marie Curie
75005, Paris, France*

² *LSPM-CNRS, Université Sorbonne Paris Nord, 99, avenue JB Clément, 93430 Villetaneuse,
France*

³ *LPA-CNRS, Ecole Normale Supérieure, PSL Research University, 75231 Paris, France*

⁴ *Department for Applied Quantum Systems, Felix Bloch Institute for Solid State Physics,
Leipzig University, 04103 Leipzig, Germany*

Abstract

Growing high-purity diamond containing dense negatively charged nitrogen-vacancy (NV⁻) centre ensembles is desirable for the development of sensitive quantum sensors that explore the coherent manipulation of the spin states of this atomic-scale defect. By using N₂O as a dopant, we demonstrate that millimetre-thick single crystals can be grown by Chemical Vapour Deposition (CVD) with substitutional nitrogen concentrations as high as 26 ppm. With a high-energy electron irradiation treatment and in-situ annealing, up to 20 % of this nitrogen can be successfully converted into NV⁻ centres leading to densities of almost 5 ppm and to a crystal displaying pink colouration and appealing optical properties. The longitudinal relaxation T₁ time in such a highly doped diamond is measured to be around 3.5 ms at 300 K while inhomogeneous dephasing time T₂^{*} is estimated to 600 ns. Despite the high NV density, Electron Spin Resonance lines are resolved with clear hyperfine splitting induced by the nuclear spin of nitrogen. The dependence of T₁ on the orientation of the magnetic field suggests that relaxation is dominated by NV-NV dipole interactions when no magnetic field is applied. Such engineered crystals constitute a promising platform for developing future quantum sensing applications.

* Corresponding author: Email: alexandre.tallaire@chimie-paristech.fr

† Corresponding author: Email: Jocelyn.achard@lspm.cnrs.fr

Keywords: quantum technologies, chemical vapour deposition, NV centres, defects, single crystal diamond

1. Introduction

Solid-state quantum systems that possess long-lived spin and/or optical coherence are highly desirable for a broad range of applications in quantum technologies (QT), from quantum networks, to information processing and quantum sensing [1]. Among them, the negatively-charged nitrogen-vacancy centre (NV⁻) in diamond is arguably one of the most promising and studied systems due to its outstanding optical and spin properties [2]. It exhibits a stable photoluminescence (PL) emission with a zero-phonon line at 637 nm, and provides a spin triplet ground level ($S = 1$) which can be initialized by optical pumping, coherently manipulated with a long coherence time (up to a few ms) through microwave excitation, and readout by pure optical means. Room-temperature optically detected Electron Spin Resonance (ESR) is indeed a key feature of the NV centre. Its spin-dependent PL has been exploited to design new generations of magnetometers that combine extreme spatial resolution with magnetic field sensitivity [3]. These sensing functionalities have also been extended to measure strain [4], electric fields [5], pressure [6] and temperature [7], that all have a direct impact on the ESR frequency.

One simple way to improve the sensitivity of such sensors is to increase the number N of sensing spins since, for NV ensembles, the shot-noise limited magnetic sensitivity η_e scales as:

$$\eta_e \propto \frac{1}{C\sqrt{NRT_2^*}} \quad (\text{eq. 1})$$

where C is the contrast of the optically-detected ESR spectrum, T_2^* denotes the inhomogeneous spin dephasing time which limits the ESR linewidth, and R is the number of detected photons that depends on collection efficiency. One important challenge is to increase the density of NV defects while maintaining good spin coherence properties [8]. This relies on the fabrication of specially engineered “*quantum grade*” synthetic crystals and mostly on the capabilities and flexibility of the plasma-assisted Chemical Vapour Deposition (CVD) technique [9–11].

Nitrogen doping efficiency and solubility in CVD diamond is however limited and obtaining high NV densities (> 10 ppb) requires that relatively large amounts of molecular nitrogen (N_2),

a typical doping gas, is added during growth, above typically 250 ppm under high plasma power density conditions [12]. However, in the presence of this impurity, a degradation of the surface morphology particularly at the edges of the crystal is usually observed [13], sometimes leading to a total loss of epitaxy. Highly N-doped CVD diamonds also contain a large amount of extended defects (dislocations and vacancy clusters in particular) that strongly reduce their optical properties, leading to a brown colouration [14,15]. An additional limitation comes from the fact that only a small fraction of the total incorporated nitrogen is in the NV form, most of it being substitutional (N_s) without an associated vacancy. A typical yield (NV/N_{total}) for untreated as-grown CVD diamonds is of the order of 1/300 [16]. Substitutional nitrogen impurities are paramagnetic defects that reduce the coherence time through dipolar coupling to the NV centre particularly at concentrations of 1 ppm and above [17]. Since high NV/N_s yields are desirable, conversion treatments through irradiation with high energy electrons, ions or laser beams followed by thermal annealing have been exploited to create and diffuse vacancies towards nitrogen impurities and thus raise the desired proportion of NVs [18].

Recently, we have shown that the use of nitrous oxide (N_2O) as a dopant in the gas phase, rather than N_2 , partially alleviates those issues by allowing higher doping levels without too much of a structural degradation of the diamond film and with improved optical properties for NV centres, in particular the suppression of photo-bleaching occurring at high excitation powers [19]. The N_2O molecule also benefits from a much lower dissociation energy in the plasma (4.6 eV instead of 9.8 eV) [20]. The presence of a low and controlled amount of oxygen next to the growing surface is expected to help etching away non-epitaxial defects, thus preserving a good morphology throughout the growth. Here we further explore the use of this dopant gas by investigating the synthesis of highly nitrogen-doped and millimetre-thick diamond films within the context of quantum technologies in which high density NV centres with good coherent properties are required. High energy electron irradiation and in-situ annealing are used to boost NV content, leading to pink diamond crystals with appealing optical properties.

2. Experimental details

A home-made high power density plasma CVD reactor was used and operated with a microwave power of 3-3.5 kW, a pressure of 200-230 mbar, a temperature of 900 °C and a methane concentration of 4 % in high purity hydrogen (9N). 500 ppm of N₂O were introduced throughout the deposition run. A High Pressure High Temperature (HPHT) type *1b* diamond (3x3 mm²) was used as a substrate. Three samples were grown under identical conditions with increasingly long deposition times and an uninterrupted growth run, leading to as-grown thicknesses of 0.7 mm (sample A), 1.7 mm (sample B) and 2.7 mm (sample C). The HPHT substrate and the edges of the crystal were then laser cut so that freestanding polished plates of 420µm, 1550µm and 2300 µm were finally obtained. Different sample thicknesses facilitate their characterization, particularly for measurements requiring analysing a transmitted light beam.

The thinnest sample (sample A) was submitted to irradiation by a 10 MeV electron beam at a fluence of $2 \times 10^{18} \text{ cm}^{-2}$ for 20 h. Throughout irradiation, the sample was heated to a temperature of 900 °C so that any vacancy formed by the impinging electrons would recombine with nitrogen impurities thus maximizing NV production while lowering the probability of forming vacancy clusters.

PL images were acquired using a *DiamondView*TM system that excites luminescence with a near bandgap UV source (225 nm). The integration time was set to 1.5 s for the as-grown sample and 0.05 s for the irradiated diamond so that fluorescence images with a good contrast are obtained. Spectroscopic characterization of the samples was carried out using a Raman/Photoluminescence (PL) system (*Renishaw InVia Raman*) using a 532 or 473 nm laser excitation line focused with a 50 × objective. FTIR analysis was performed in transmission with a *Bruker Tensor 27* system. The freestanding diamond plates were attached to a pierced holder and 256 scans were acquired between 400 and 4000 cm⁻¹. The resolution was around 2 cm⁻¹. The absorption coefficient was normalized so that it reaches 12.8 cm⁻¹ at 2000 cm⁻¹ which is the expected value for diamond [21]. Ultraviolet-visible (UV-Vis) absorption spectrometry was performed in transmission using a *Carry 6000i* spectrophotometer in the range 200-800 nm with steps of 0.25 nm either at room temperature or in a closed cycle helium cryostat maintained at a temperature of 77 K. A reflection loss spectrum was subtracted to get the real absorption coefficient from the sample. Since reflection losses may be greater than expected

from this simple model, we slightly shifted the data in order to get zero absorption at a wavelength of 700 nm.

High resolution spectroscopy measurements were performed using a home-built confocal system. It consists of a laser source delivering a maximum of 5 mW at 532 nm, the intensity of which is controlled by an Acousto-Optic Modulator (AOM). The laser is passing through a dichroic mirror and sent to a microscope objective (with a numerical aperture of 0.6) that focusses the laser onto the sample and collects the photoluminescence. Most of the PL then goes back through the dichroic mirror (which reflects light at a wavelength above 638 nm) and is mode matched to a multimode fibre that is directly connected to an Avalanche Photodiode (*Perkin Elmer*). For the spin resonance measurements, we use a home-made free-space antenna loop driven by a microwave function generator (*Rohde and Schwarz*) and a permanent magnet for Zeeman splitting the four NV spins classes.

3. Results and discussion

3.1. As grown CVD diamond with N₂O doping

Images of the 3 freestanding CVD samples (A, B and C) grown with addition of 500 ppm of N₂O are presented in Fig. 1a. One can notice that they exhibit brown colouration typical for diamonds of that thickness and doping range [22,23]. It is however noticeable that despite the high added amount of N₂O thick single crystalline material could be successfully produced whereas a sample grown with similar growth conditions and addition of N₂ would lead to a polycrystalline or highly defective film. The transmitted light under cross-polarizers shown here for sample A (Fig. 1b) evidences a typical cross-shape pattern resulting from the dislocation network generated in CVD-grown material [24] with a typical density of 10⁵-10⁶ cm⁻². Under the UV-light of the *DiamondView*TM (Fig. 1c-e), the samples display bright red-yellow fluorescence indicative of the presence of NV centres. A 1.5 s integration time was used here to acquire the images. Despite having been “scaif”-polished to a low roughness, the fingerprint of growth features at the top surface (round shape hillocks) is revealed under UV-light due to local variation of nitrogen doping in the crystal (Fig. 1c and d) [25]. No evidence of strong internal stress that would show-up as bright blue fluorescence was found. In addition, the side of sample C (Fig. 4e) examined under the *DiamondView*TM shows a rather uniform

colouration although layering is visible. This originates from local variation of the NV density induced by temperature drifts that were compensated and that we estimate to around $\pm 30^\circ\text{C}$ during the deposition run. Lower temperatures are indeed known to lead to higher NV incorporation efficiency [26].

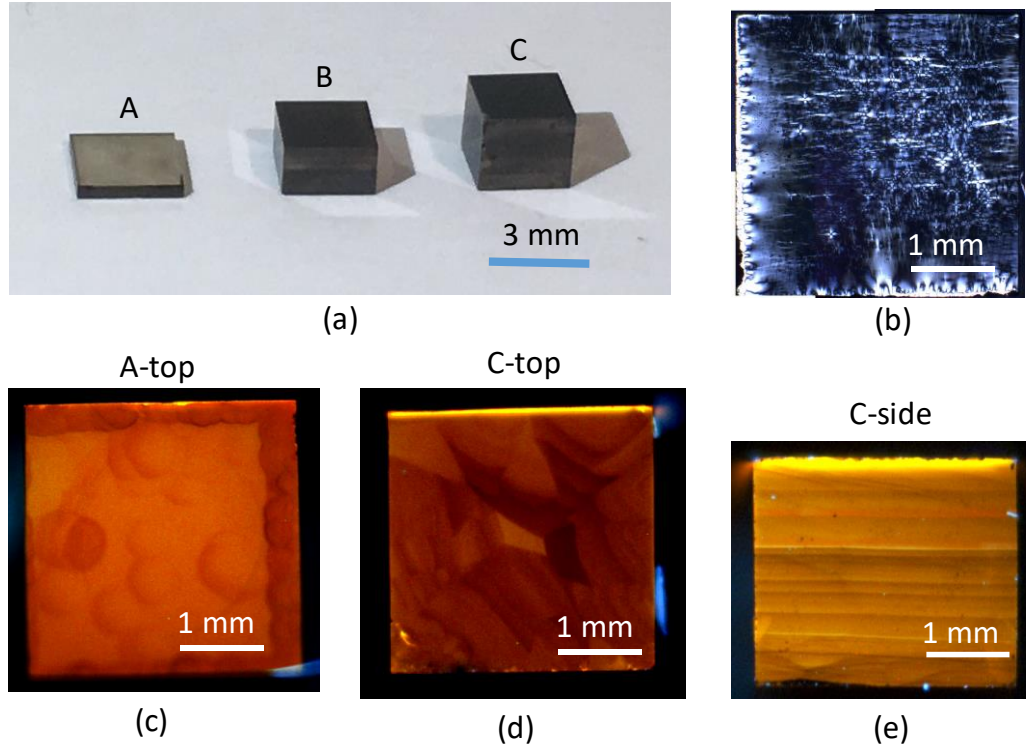


Fig. 1. (a) Images of the 3 CVD-grown samples. A: 420 μm -thick, B: 1550 μm -thick and C: 2300 μm -thick. (b) Image of sample A in transmission under cross-polarizers showing dislocation-related patterns. (c)-(e) DiamondViewTM PL images of samples A and C acquired with a 1.5 s integration time either on the top surface or on the side surface (i.e. perpendicularly to the growth direction).

Raman/PL analysis was carried out under both 473 and 532 nm excitation in a non-confocal system (Fig. 2a and 2b). Strong emission from NV^0 and NV^- centres is evidenced when comparing with the intensity from the diamond Raman peak (labelled R on Fig. 2). For an excitation line at 532 nm, emission from NV^- dominates as compared to that from NV^0 due to different absorption cross-section at different wavelengths [27]. With an excitation at 473 nm, a slight contribution starting at 503 nm and extending up to 525 nm at the base of the Raman peak is believed to be related to the H3 centre, an aggregated nitrogen defect (N-V-N). We found no evidence of SiV centre that would otherwise show up at 737 nm. The FWHM of the

diamond Raman peak was found to be around 5 cm^{-1} at 473 nm which is broader than that typically measured for highly pure CVD films ($1.5 - 1.7 \text{ cm}^{-1}$). Such a broadening is probably induced by the presence of impurities and vacancy clusters (i.e. disorder) in the crystal.

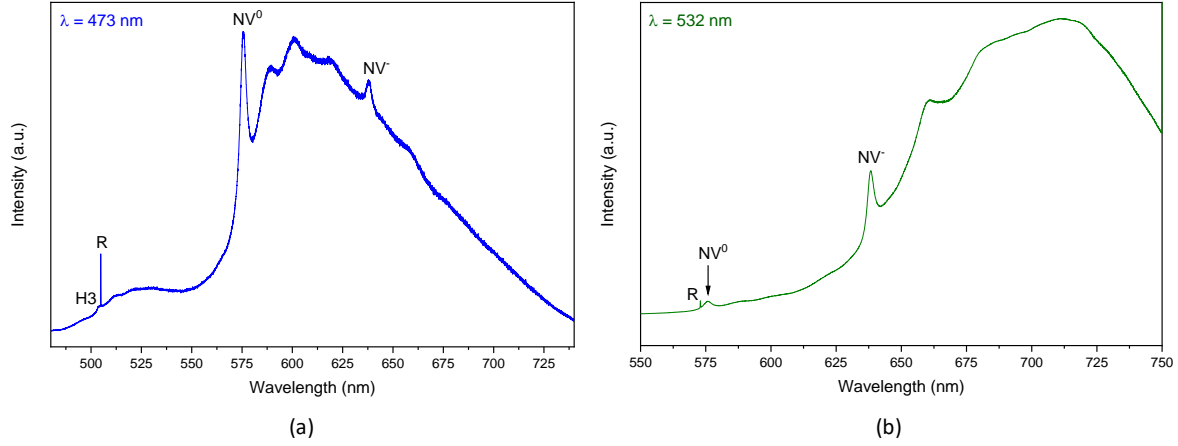


Fig. 2. PL spectra of as-grown freestanding CVD diamond with N_2O addition (sample A) under (a) 473 nm and (b) 532 nm excitation lines respectively. The diamond Raman peak is labelled R and the main emissions are indicated.

FTIR analysis was then carried out to assess nitrogen incorporation. The spectrum of Fig. 3 (sample B) reveals the typical multi-phonon absorption of diamond between 1600 and 2600 cm^{-1} . Absorption in the one-phonon region (below 1332 cm^{-1}) is not permitted in a perfect diamond but is induced by defects that locally modify the symmetry and introduce distortion. The intensity of the 1130 cm^{-1} band (inset of Fig. 3a) can be used to evaluate the amount of substitutional nitrogen in their neutral charge state (N_s^0) while that at 1332 cm^{-1} is proportional to N_s^+ concentration [20]. Based on this, we estimate 18 and 8 ppm of N_s^0 and N_s^+ respectively, leading to a total substitutional nitrogen concentration of about 26 ± 5 ppm. This is a doping efficiency of about 5×10^{-2} and a considerable amount of nitrogen for a CVD-grown diamond in which doping levels rarely go beyond 1 ppm in high-quality single crystals unlike HPHT type *1b* crystals that can contain several hundreds of ppm [28]. The proportion of neutrally charged nitrogen represents here around 70 % of the total substitutional nitrogen, a fairly high value. According to a recent study [29], it suggests that the amount of acceptor defects was low, a good indicator of the final performance of the material in quantum applications. We note that long-time exposure to UV irradiation of the sample prior to

measurement was not performed although this treatment is known to maximize the proportion of N_s^0 respectively to N_s^+ . The value of 70 % might thus be underestimated here.

Additional peaks in the FTIR spectrum at 1046, 1353 and 1371 cm^{-1} are similar to those already reported by Wang et al and Zaitsev et al. [30–32] in nitrogen-doped CVD diamonds. The presence of hydrogen impurities is also evidenced from the CH stretch vibrations at higher wavenumbers (2600-3000 cm^{-1}) [33], as well as the presence of a peak at 3123 cm^{-1} from NVH^0 defects. We estimate a concentration of NVH^0 of about 0.3 ppm from the area of its absorption [34]. Absorption at 3324 cm^{-1} is related to substitutional nitrogen decorated by a hydrogen atom ($N_s:H-C^0$) [35]. Hydrogen is a commonly found impurity in CVD-grown diamonds especially those grown at high growth rates which is the case when nitrogen is intentionally added.

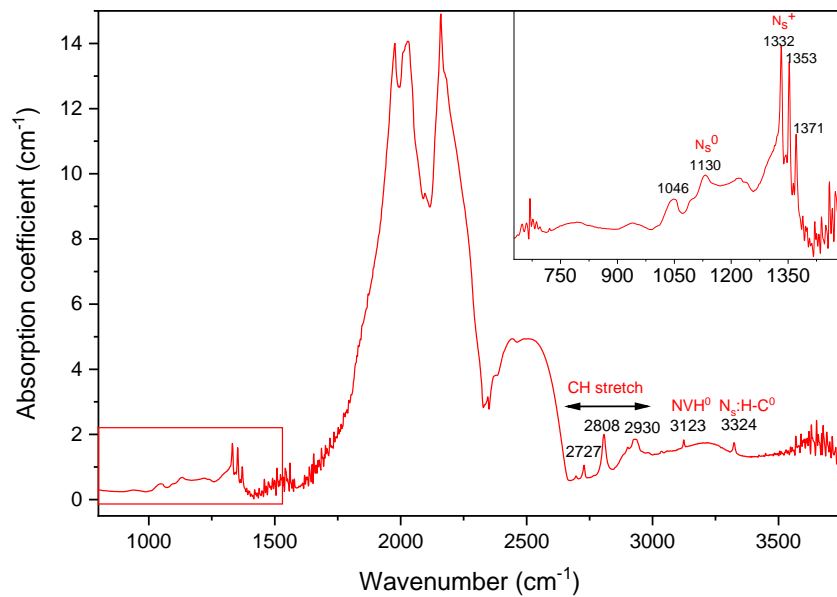


Fig. 3. FTIR spectrum of a freestanding CVD diamond grown with N_2O addition (sample B). The inset shows a zoom into the red squared area.

UV-Vis absorption measurements acquired at room temperature are presented in Fig. 4 for the thinnest sample (sample A). The presence of a strong absorption band at 270 nm corresponds to electronic transitions from the valence band to N_s^0 . Its intensity is consistent with the 26 ppm nitrogen doping level calculated previously by FTIR [36]. The brownish colouration of the sample is attributed to the presence of a continuum absorption from 500 nm to the deep UV, as well as 2 broad bands observed at 510 and 350 nm. They are related

to defects other than substitutional nitrogen, such as vacancy clusters [37] or even possibly sp^2 carbon nanoclusters [38] that were generated during growth. We note though that those bands have rather moderate absorption coefficients as compared to that originating from substitutional nitrogen. This further supports the fact that growth with N_2O provides a way to generate a high nitrogen doping while limiting the amount of other defects in the crystal. Looking at the 550-650 nm region (inset of Fig. 4), the presence of a weak peak from NV^- centres at 637 nm is detected together with unattributed absorptions at 624 and 598 nm. UV-Vis absorption was also performed at low temperature (77 K) on sample B (not presented here). Under those conditions, the density of NV centres is proportional to the area of the absorption peak [39]. We estimated a concentration of 0.1 ppm of NV^- whereas NV^0 absorption was not detected suggesting that its concentration was of the order of 0.01 ppm or below. The strong proportion of negatively charged defects with respect to neutral ones is typical of the presence of a high amount of nitrogen that acts as an efficient electron donor. No peaks related to isolated vacancies (V^0 or V^- at 741 nm and 393 nm respectively) were found in the as-grown samples.

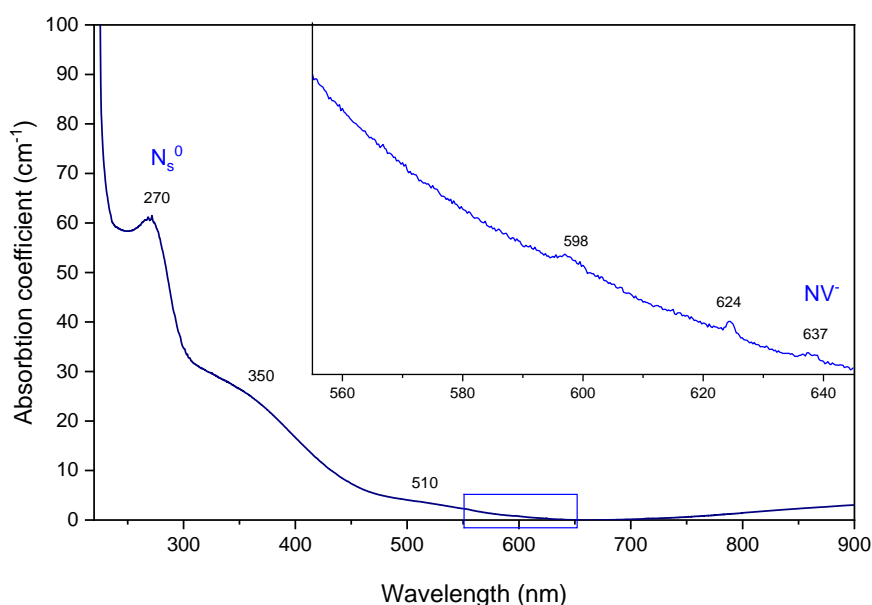


Fig. 4. Room temperature UV-Vis optical absorption of an as-grown freestanding CVD diamond (sample A) grown with 500 ppm of N_2O . The inset shows a zoom into the blue squared area.

3.2. Irradiated pink CVD diamond

Sample A was irradiated with 10 MeV electrons and in-situ annealed at 900 °C. In this energy range, electrons' penetration depth is larger than the thickness of the film leading to uniform creation of vacancies throughout the diamond crystal. The irradiation fluence of $2 \times 10^{18} \text{ cm}^{-2}$ was chosen so that the vacancies' density (expected to be $7 \times 10^{18} \text{ cm}^{-3}$) [40] is comparable to the nitrogen concentration in the crystal (around 26 ppm i.e. $5 \times 10^{18} \text{ cm}^{-3}$). This approach aims at maximizing N_s to NV conversion by diffusion and capture of vacancies. As a result of the irradiation, the sample exhibited a bright pink colouration visible in Fig. 5a. Under the 473 nm laser beam of the Raman microscope the bright red emission from NV centres was obvious (Fig. 5b). When observed again under the *DiamondView*TM, the top surface of the sample still displayed the same red fluorescence with a visible growth pattern. However, the acquisition time was reduced from 1.5 s to 0.05 s to obtain an image with roughly similar brightness. This $30 \times$ increase in fluorescence intensity gives a first hint into the strong increase in the number of NVs produced.

Room temperature PL/Raman analysis was then performed using either 473 or 532 nm laser excitation. The very high emission intensity originating from NV centres can be judged by comparing with the respectively low intensity of the diamond Raman peak in the insets of Fig. 6a and Fig. 6b. Using the green laser, the Raman contribution is even completely overlapped with the NV^0 band. Again no contribution from SiV^- centres expected at 737 nm was detected. This suggests that the silicon background contamination in our sample was relatively low since we expect this negative charge state of the defect to be promoted under high nitrogen content [41]. No contribution from the radiation-induced GR1 centre at 741 nm (V^0) [36] was found in PL which indicates that no excess vacancies were produced by the irradiation and that the majority was captured by impurities. Interestingly, emission from the H3 centre (N-V-N) [36] around 503 nm was enhanced whereas it was just barely visible before irradiation. Since nitrogen atoms are not mobile at the annealing temperatures that were used, we conclude that not all nitrogen in the sample was in the form of single substitutional N_s defects but nitrogen pairs were likely to be present too. Vacancies diffused and trapped by those aggregates were formed after irradiation, leading to the observed enhancement of the H3 centre. Consequently, the total nitrogen concentration is probably higher than that simply estimated from the previous N_s measurement.

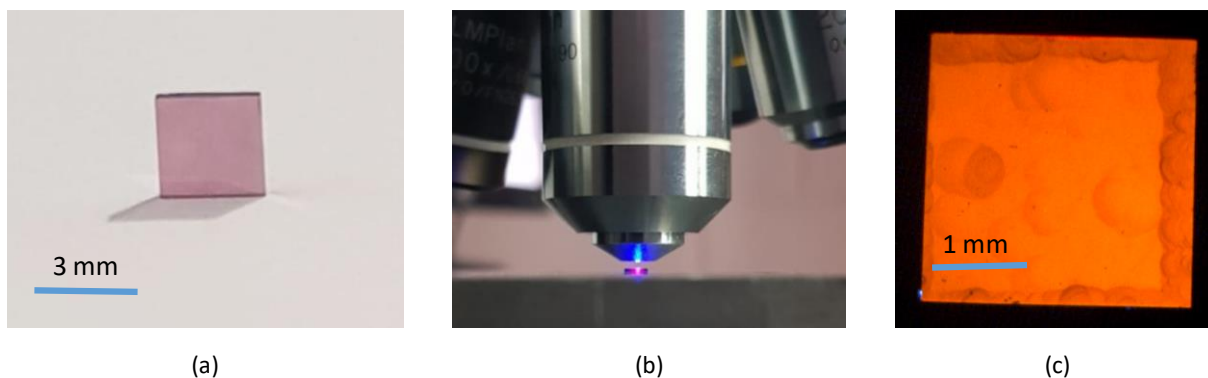


Fig. 5. CVD diamond sample A after electron irradiation and in-situ annealing. (a) Optical image showing the pink colouration. (b) Bright red luminescence observed under blue laser illumination. (c) DiamondView™ image of the top surface using an integration time of 0.05 s.

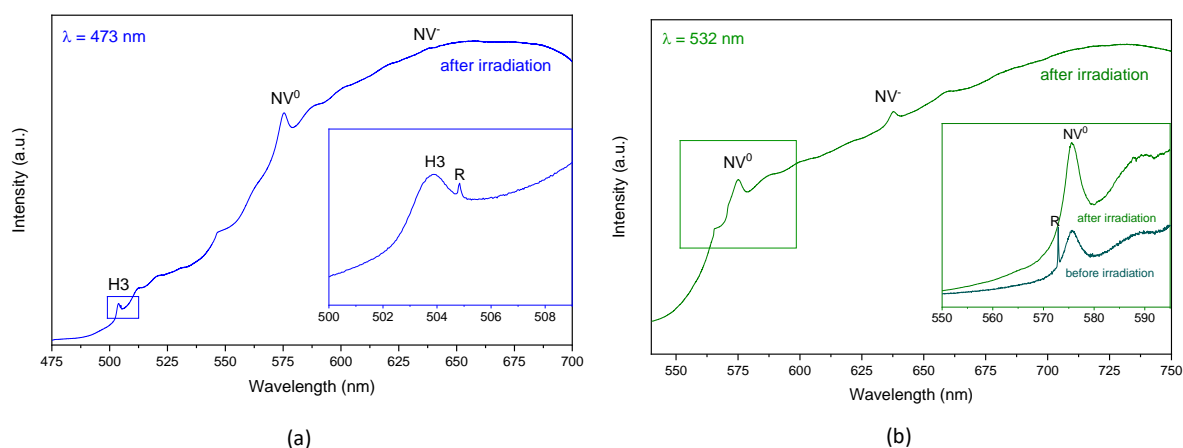


Fig. 6. PL-Raman analysis of CVD diamond sample A after electron irradiation and in-situ annealing under (a) 473 nm and (b) 532 nm excitation lines respectively. The diamond Raman peak is labelled R and the main emissions are indicated. The inset in (a) shows a zoom into the blue squared area. The inset in (b) shows a zoom into the green squared area. The spectrum of the sample before irradiation is provided as a comparison for (b).

FTIR spectroscopy of the irradiated and in-situ annealed sample A presented in Fig. 7 brings further information on the nitrogen content. We observed that absorption in the one-phonon region was extremely low leading to a noisy contribution between 800 and 1500 cm^{-1} even after long acquisition times. The previous peaks at 1130 and 1332 cm^{-1} could no longer be detected indicating a drastic drop in the concentration of isolated substitutional nitrogen. This is consistent with the fact that N_s were successfully converted into NVs by the treatment. On the other hand, the 3123 cm^{-1} peak (NVH^0) was strongly increased whereas the CH stretch

contributions decreased accordingly. From the area of the absorption [39], we calculated that the density of NVH^0 was as high as 0.8 ppm. A significant fraction of the available nitrogen was thus passivated by hydrogen and unavailable to create the desired NV^- centres. Besides, the intensity of the 3324 cm^{-1} peak related to a substitutional nitrogen associated to a hydrogen atom ($\text{N}_\text{s}\text{:H-C}^0$) also increased by almost a factor of 5. Since such complexes are stable, they constitute another path to the loss of available nitrogen. These results indicate that the diffusion and capture of vacancies as well as possibly the diffusion of hydrogen atoms [42] led to such a drastic modification of the defect content in the crystal.

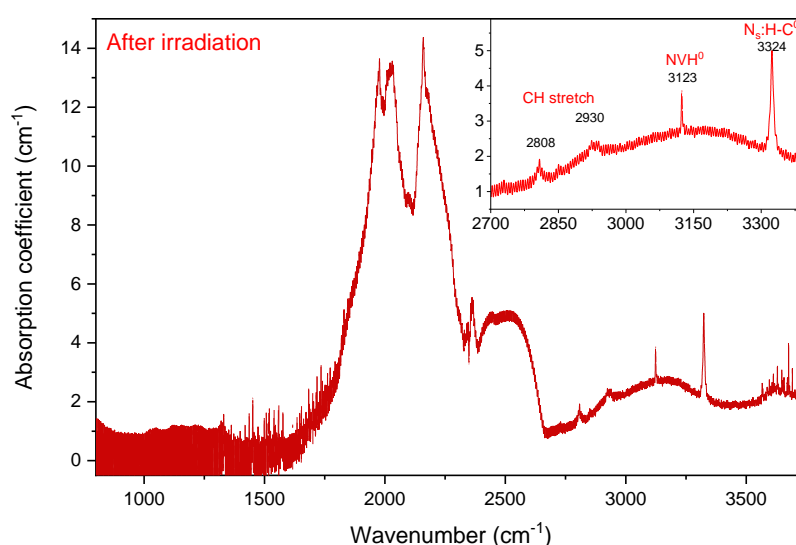


Fig. 7. FTIR spectrum of CVD diamond sample A after electron irradiation and in-situ annealing. The inset shows a zoom into the red squared area where specific defects are indicated.

Reorganisation in the distribution of impurities induced by the irradiation/annealing treatment is also clearly apparent in the room temperature UV-Vis absorption spectroscopy results presented in Fig. 8 in which absorption of the sample before and after irradiation is compared to that from a pure (undoped) CVD film of similar thickness. The absorption is dominated by that originating from NV centres with two clear lines at 575 and 637 nm as well as a broad phonon-related absorption band. The contribution from N_s^0 at 270 nm is overlapped by unknown contributions at 286 and 266 nm and can no longer be clearly identified. This supports again the efficient conversion of substitutional nitrogen into NV

centres. The presence of two regions with low absorption in the blue (around 450 nm) and at a wavelength above 640 nm is responsible for the pink colouration of this sample [31].

To further quantify the amount of impurities, we acquired UV-Vis absorption spectroscopy at low temperature (77 K). From the area of the absorption peaks presented in Fig. 9. and using the calibration constants reported in [43] and [36], we estimated NV^0 and NV^- concentrations to 2.3 and 4.6 ppm respectively. This corresponds to a high conversion efficiency of 20 %. The presence of remaining vacancies but in a low amount was evidenced by very weak absorptions at 3.15 eV (393.5 nm, V^-) and 1.67 eV (741 nm, V^0). They were quantified to 55 ppb and 20 ppb respectively. No large excess of vacancies was produced in agreement with the PL results. An additional peak at 595 nm already reported in irradiated nitrogen-doped diamonds is relatively pronounced [36], as well as narrow absorptions at 446.5 and 424.5 nm. Such defects might be related to interstitials or vacancy clusters that were not completely annealed out.

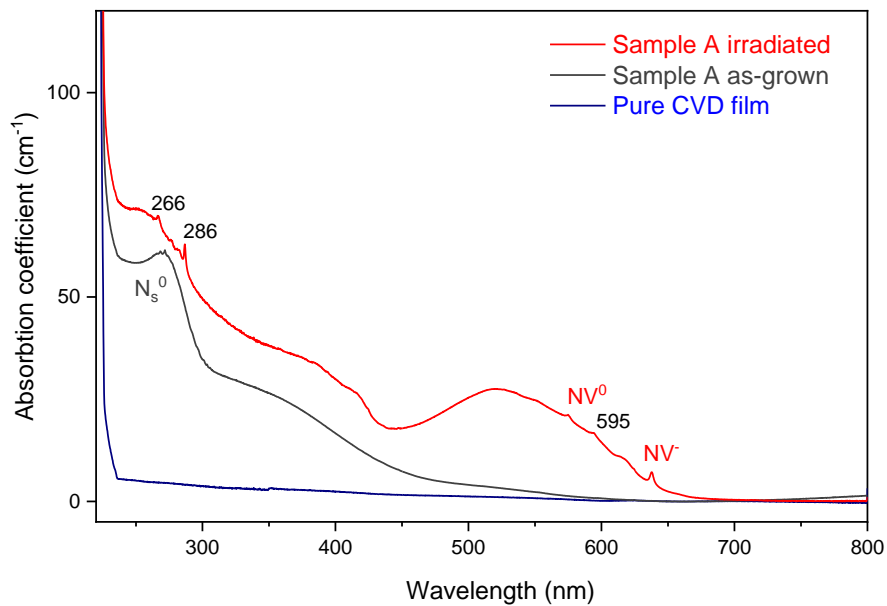


Fig. 8. Room temperature UV-Vis optical absorption of CVD diamond sample A after electron irradiation and in-situ annealing (red trace) compared to that acquired before irradiation (grey trace) as well as an undoped freestanding CVD plate of similar thickness used as a reference (blue trace).

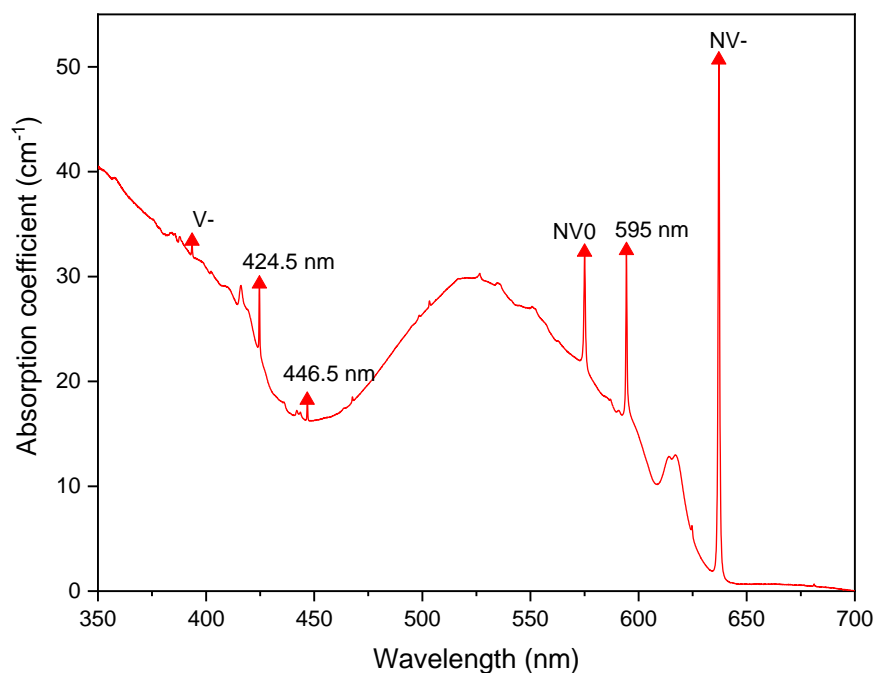


Fig. 9. Low temperature (77 K) UV-Vis optical absorption of CVD diamond sample A after electron irradiation and in-situ annealing.

A summary of the results on the defect quantification after the treatment based on the different characterization techniques is presented in Table 1. One can see the redistribution in the nature and density of defects that occurred.

Table 1. Quantification of main defects before and after irradiation of the sample grown with 500 ppm of N₂O in the gas phase. N.Q. refers to “not quantifiable”.

Defect	As grown with 500 ppm N ₂ O	After electron irradiation/annealing	Measurement technique
NV ⁻	0.1 ppm	4.6 ppm	UV-Vis (637 nm)
NV ⁰	< 10 ppb	2.3 ppm	UV-Vis (575 nm)
V ⁰	N.Q.	55 ppb	UV-Vis (741 nm)
V ⁻	N.Q.	20 ppb	UV-Vis (393.5 nm)
N _s ⁰	18 ppm	N.Q.	FTIR (1130 cm ⁻¹)
N _s ⁺	8 ppm	N.Q.	FTIR (1332 cm ⁻¹)
NVH ⁰	0.3 ppm	0.8 ppm	FTIR (3123 cm ⁻¹)

3.3. Spin properties of NV centres in as-grown and irradiated CVD diamonds

In order to assess the properties of NV centres in the CVD diamonds grown with N₂O addition, time-resolved spectroscopy measurements were carried out on both the as-grown and irradiated samples. In the as-grown sample (B), the spin T_1 times were measured using pulses of green laser light separated by a varying time τ . The photoluminescence was extracted during the first 10 μ s of the second pulse as shown in Fig. 10a (sequence 1). In heavily doped samples however, it has been noticed [44] that photoionisation can modify the extracted PL change as a function of time due to recombination of NV⁰ back to NV⁻ centers in the dark when excited with green laser powers above 10 μ W. To estimate T_1 on this sample, it is thus necessary to perform an extra measurement with two green laser pulses interleaved by a short microwave π pulse (sequence 2 of Fig. 10a). Here we apply a 100 ns microwave pulse at the zero-field splitting of 2.87 GHz immediately after the first pulse. We then subtract the two curves of sequence 1 and 2 and obtain the curve shown in Fig. 10a. This standard rejection technique removes this artefact and measures the true relaxation from the $m_s = \pm 1$ spin states, which we found to be $T_1 = 3.6$ ms after fitting with an exponentially decaying curve. This value is consistent with the typical spin-lattice relaxation times at ambient conditions [45]. For the as-grown sample, the relaxation does not depend on the external magnetic field for up to 200 G.

The situation is very different for the irradiated sample (A). There, only a slight modification of the decay curve was seen due to photoionisation effects, at powers below 100 μ W suggesting that the presence of substitutional nitrogen in the as-grown sample indeed assists the NV⁰ to NV⁻ recombination in the dark [15]. In the irradiated sample, at powers above 100 μ W, only a slight initial increase of the PL is observed. We thus chose to operate at lower power in order not to use the rejection technique. In this sample however, the relaxation time was observed to depend critically on the magnetic field strength and orientation. As it was observed already in [46] when some classes of NV centers are degenerate, the dipole-dipole interaction can cause faster spin-relaxation thus reducing the T_1 time. Trace i) of Fig. 10b shows a T_1 curve taken with a magnetic field along an arbitrary direction where no degeneracy occurs (the corresponding electron-spin-resonance is shown as a blue trace in the inset). In this case we measured a decay time of 3.5 ms close to the value measured in the as-grown sample B. This suggests that phonons are the dominant relaxation

mechanism here too. Now, we tune the magnetic field to the [100] direction so that all NV centers' classes are degenerate. A single ESR line then appears in the spectrum (see green trace in the inset) and the relaxation is faster (trace ii)). Using an exponential fit still gives a good agreement with the data [46]. We measured a relaxation time of 2.2 ms, lower than the phonon-limited T_1 . The dipole-dipole interaction then becomes dominant in this regime showing again the very high NV centers density of the irradiated sample.

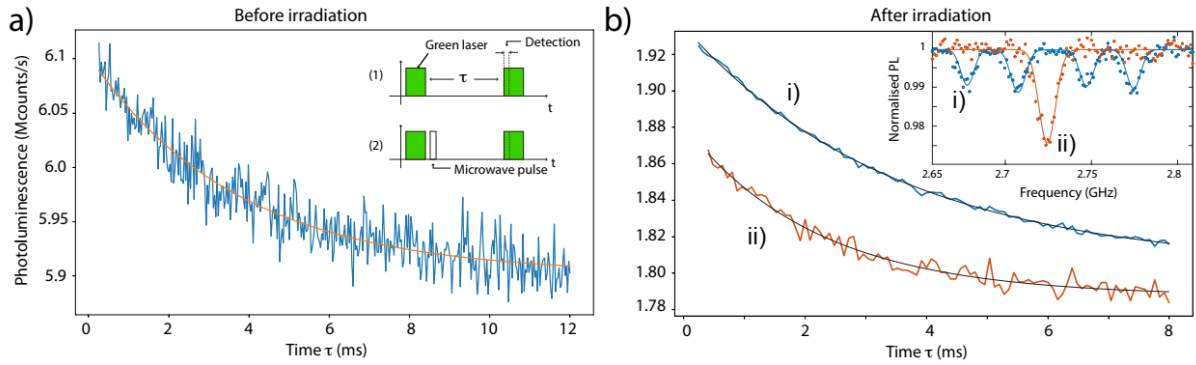


Fig. 10. a) Longitudinal relaxation of the NV spin population (T_1 time) in sample B (not irradiated). The curve is the subtraction of the data obtained in the sequences shown in the inset. The sequence (2) is used to remove the background contribution from NV ionisation in the T_1 measurement. b) Longitudinal relaxation of the NV spin population (T_1 time) in irradiated sample A under two different orientation of the magnetic field: i) arbitrary orientation, ii) orientation along the [100] direction. The inset shows the corresponding ESR spectra.

The ESR spectra of both the as-grown (B) and irradiated (A) samples are sufficiently narrow to allow resolving the hyperfine structure induced by coupling to the nuclear spin of nitrogen and leads to the appearance of a triplet of resonances (Fig. 11b). This indicates that the highly-doped sample has a low amount of defects and good crystalline quality that limits broadening of the lines. T_2^* times were estimated by scanning the frequency of a microwave signal across one of the spin resonances at very low power in order not to saturate the transition. In this condition, the linewidth is then determined by the T_2^* time [47]. We found similar values of about 600 ns for both samples (A irradiated and B as grown). We note that the T_2^* values measured here would correspond to those reported for samples having nitrogen concentrations of the order of 20 ppm (see reference [48]) which is in good agreement with our previous estimation. It is striking that the T_2^* values remained roughly the same after irradiation which indicates that one can benefit from the high brightness of a

dense NV ensemble without any trade off on the coherence time. Thus the $[NV^-] \times T_2^*$ product, a figure of merit for NV sensing applications, is of the order of $3 \mu s.ppm$, a favourable value as indicated by a recent report [29].

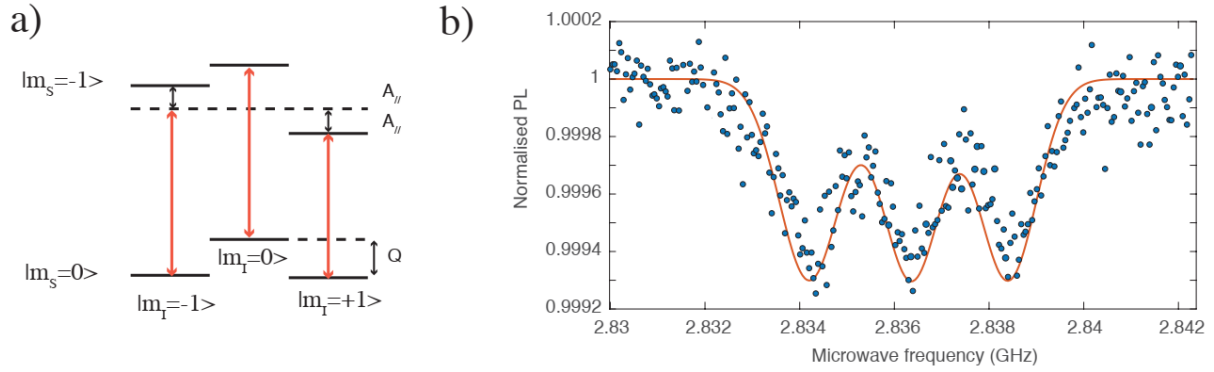


Fig. 11 (a) Energy level scheme of the NV centre showing the 3 main transitions due to hyperfine splitting induced by ^{14}N . (b) Electronic spin resonance spectrum on one of the NV orientations in the irradiated sample (A).

Conclusion

Diamond crystals with a high density of luminescent NV centres (of the order of 1 ppm or more) and presenting good coherence properties are highly desired for applications in quantum sensing for which they may advantageously extend the performance and sensitivity of the foreseen devices. Obtaining high NV concentrations in CVD-grown diamonds is however hampered by the low solubility of nitrogen, the poor N_s/NV yield and the deleterious effect of N_2 doping gas on the surface morphologies of the films. By using N_2O as a doping source during growth, millimetre-thick diamond crystals with high crystalline quality were successfully produced. Nitrogen levels as high as 26 ppm were measured which represents a significant amount for a CVD-grown diamond. The as-grown crystal exhibited a slightly brownish colouration due to absorption by N_s at 270 nm and an increasing absorption at wavelengths below 500 nm. A moderate fraction of NV^- centres of about 100 ppb was measured. By irradiating with high energy electrons (10 MeV) and in-situ annealing the samples at 900 °C, substitutional nitrogen was efficiently converted into NV with a yield of about 20 % leading to highly dense NV centre ensembles (almost 5 ppm). A pink diamond crystal with appealing optical properties was then obtained. Passivation of part of the defects by hydrogen leading

to the formation of NVH centres at a concentration level comparable to NVs was evidenced and constitute a possible limitation.

The relaxation time T_1 of the irradiated sample indicates a dependence on the orientation of the magnetic field unlike the as-grown sample. Shorter T_1 times were indeed obtained when the different NV populations are degenerate and experience a similar magnetic field projection along their axis, i.e. when their resonance frequencies match. This suggests that in such highly dense NV ensembles, dipolar interaction between NV centres is an important limiting mechanism in addition to phonon-assisted relaxation. Fairly long T_2^* times of 600 ns were measured and were not decreased by the irradiation treatment, which indicates that one can benefit from a high NV density without compromising their spin properties. Such specially engineered pink diamond crystals with dense NV ensembles constitute a milestone towards the development of quantum sensors and devices with improved performance.

Acknowledgements:

This project has received funding from the European Union's research and innovation program through the Project ASTERIQS under grant agreement n° 820394 and through the QUANTERA project MICROSENS n° ANR-18-QUAN-0008-02. It has been also supported by Region Ile-de-France in the framework of DIM SIRTEQ. ANR (Agence Nationale de la Recherche) and CGI (Commissariat à l'Investissement d'Avenir) are also gratefully acknowledged for their financial support through Labex SEAM (Science and Engineering for Advanced Materials and devices), ANR-10-LABX-096 and ANR-18-IDEX-0001, the Diamond-NMR project n° ANR-19-CE29-0017-04 and the SADAHPT project n° ANR-19-CE30-0027-02.

- [1] A. Acín, I. Bloch, H. Buhrman, T. Calarco, C. Eichler, J. Eisert, D. Esteve, N. Gisin, S.J. Glaser, F. Jelezko, S. Kuhr, M. Lewenstein, M.F. Riedel, P.O. Schmidt, R. Thew, A. Wallraff, I. Walmsley, F.K. Wilhelm, The quantum technologies roadmap: a European community view, New J. Phys. 20 (2018) 080201. <https://doi.org/10.1088/1367-2630/aad1ea>.

- [2] M.W. Doherty, N.B. Manson, P. Delaney, F. Jelezko, J. Wrachtrup, L.C.L. Hollenberg, The nitrogen-vacancy colour centre in diamond, *Phys. Rep.* 528 (2013) 1–45.
<http://dx.doi.org/10.1016/j.physrep.2013.02.001>.
- [3] L. Rondin, J.P. Tetienne, T. Hingant, J.-F. Roch, P. Maletinsky, V. Jacques, Magnetometry with nitrogen-vacancy defects in diamond, *Rep. Prog. Phys.* 77 (2014) 056503.
- [4] M. E. Trusheim, D. Englund, Wide-field strain imaging with preferentially aligned nitrogen-vacancy centers in polycrystalline diamond, *New J. Phys.* 18 (2016) 123023.
- [5] F. Dolde, H. Fedder, M.W. Doherty, T. Nöbauer, F. Rempp, G. Balasubramanian, T. Wolf, F. Reinhard, L.C.L. Hollenberg, F. Jelezko, J. Wrachtrup, Electric-field sensing using single diamond spins, *Nat. Phys.* 7 (2011) 459–463. <https://doi.org/10.1038/nphys1969>.
- [6] M.W. Doherty, V.V. Struzhkin, D.A. Simpson, L.P. McGuinness, Y. Meng, A. Stacey, T.J. Karle, R.J. Hemley, N.B. Manson, L.C.L. Hollenberg, S. Prawer, Electronic Properties and Metrology Applications of the Diamond NV- Center under Pressure, *Phys. Rev. Lett.* 112 (2014) 047601.
- [7] G. Kucsko, P.C. Maurer, N.Y. Yao, M. Kubo, H.J. Noh, P.K. Lo, H. Park, M.D. Lukin, Nanometre-scale thermometry in a living cell, *Nature*. 500 (2013) 54–58.
<https://doi.org/10.1038/nature12373>.
- [8] T. Wolf, P. Neumann, K. Nakamura, H. Sumiya, T. Ohshima, J. Isoya, J. Wrachtrup, Subpicotesla Diamond Magnetometry, *Phys. Rev. X*. 5 (2015) 041001.
<https://doi.org/10.1103/PhysRevX.5.041001>.
- [9] R.S. Balmer, J.R. Brandon, S.L. Clewes, H.K. Dhillon, J.M. Dodson, I. Friel, P.N. Inglis, T.D. Madgwick, M.L. Markham, T.P. Mollart, N. Perkins, G.A. Scarsbrook, D.J. Twitchen, A.J. Whitehead, J.J. Wilman, S.M. Woollard, Chemical vapour deposition synthetic diamond: materials, technology and applications, *J. Phys. Condens. Matter*. 21 (2009) 364221.
- [10] A. Tallaire, J. Achard, F. Silva, O. Brinza, A. Gicquel, Growth of large size diamond single crystals by plasma assisted chemical vapour deposition: Recent achievements and remaining challenges, *Comptes Rendus Phys.* 14 (2013) 169–184.
- [11] T. Teraji, T. Yamamoto, K. Watanabe, Y. Koide, J. Isoya, S. Onoda, T. Ohshima, L.J. Rogers, F. Jelezko, P. Neumann, J. Wrachtrup, S. Koizumi, Homoepitaxial diamond film

growth: High purity, high crystalline quality, isotopic enrichment, and single color center formation, *Phys. Status Solidi A*. 212 (2015) 2365–2384.
<https://doi.org/10.1002/pssa.201532449>.

- [12] J. Achard, F. Silva, O. Brinza, A. Tallaire, A. Gicquel, Coupled effect of nitrogen addition and surface temperature on the morphology and the kinetics of thick CVD diamond single crystals, *Diam. Relat. Mater.* 16 (2007) 685–689.
- [13] Y. Meng, C. Yan, S. Krasnicki, Q. Liang, J. Lai, H. Shu, T. Yu, A. Steele, H. Mao, R.J. Hemley, High optical quality multicarat single crystal diamond produced by chemical vapor deposition, *Phys. Status Solidi A*. 209 (2012) 101–104.
<https://doi.org/10.1002/pssa.201127417>.
- [14] I. S. Godfrey, U. Bangert, A Study of the relationship between brown colour and extended defects in diamond using core-loss electron energy loss spectroscopy, *J. Phys. Conf. Ser.* 371 (2012) 012016.
- [15] R.U.A. Khan, B.L. Cann, P.M. Martineau, J. Samartseva, J.J.P. Freeth, S.J. Sibley, C.B. Hartland, M.E. Newton, H.K. Dhillon, D.J. Twitchen, Colour-causing defects and their related optoelectronic transitions in single crystal CVD diamond, *J. Phys. Condens. Matter.* 25 (2013) 275801.
- [16] A.M. Edmonds, U.F.S. D’Haenens-Johansson, R.J. Cruddace, M.E. Newton, K.M.C. Fu, C. Santori, R.G. Beausoleil, D.J. Twitchen, M.L. Markham, Production of oriented nitrogen-vacancy color centers in synthetic diamond, *Phys. Rev. B*. 86 (2012) 035201.
- [17] N. Bar-Gill, L.M. Pham, C. Belthangady, D. Le Sage, P. Cappellaro, J.R. Maze, M.D. Lukin, A. Yacoby, R. Walsworth, Suppression of spin-bath dynamics for improved coherence of multi-spin-qubit systems, *Nat Commun.* 3 (2012) 858.
- [18] J.M. Smith, S.A. Meynell, J.A.C. Bleszynski, J. Meijer, Colour centre generation in diamond for quantum technologies, *Nanophotonics*. 8 (2019) 1889–1906.
<https://doi.org/10.1515/nanoph-2019-0196>.
- [19] A. Tallaire, L. Mayer, O. Brinza, M. A. Pinault-Thaury, T. Debuisschert, J. Achard, Highly photostable NV centre ensembles in CVD diamond produced by using N₂O as the doping gas, *Appl. Phys. Lett.* 111 (2017) 143101. <https://doi.org/10.1063/1.5004106>.

- [20] L. Date, K. Radouane, H. Caquineau, B. Despax, J.P. Couderc, M. Yousfi, Analysis of the N₂O dissociation by r.f. discharges in a plasma reactor, *Surf. Coat. Technol.* 116–119 (1999) 1042–1048. [https://doi.org/10.1016/S0257-8972\(99\)00287-X](https://doi.org/10.1016/S0257-8972(99)00287-X).
- [21] C. Hartland, A study of point defects in CVD diamond using electron paramagnetic resonance and optical spectroscopy, PhD dissertation, University of Warwick, 2014. <http://webcat.warwick.ac.uk/record=b2754901~S1>.
- [22] S.J. Charles, J.E. Butler, B.N. Feygelson, M.E. Newton, D.L. Carroll, J.W. Steeds, H. Darwish, C.S. Yan, H.K. Mao, R.J. Hemley, Characterization of nitrogen doped chemical vapor deposited single crystal diamond before and after high pressure, high temperature annealing, *Phys. Status Solidi A.* 201 (2004) 2473–2485.
- [23] Y. Meng, C. Yan, J. Lai, S. Krasnicki, H. Shu, T. Yu, Q. Liang, H. Mao, R.J. Hemley, Enhanced optical properties of chemical vapor deposited single crystal diamond by low-pressure/high-temperature annealing, *Proc. Natl. Acad. Sci.* 105 (2008) 17620–17625. <https://doi.org/10.1073/pnas.0808230105>.
- [24] A. Tallaire, T. Ouisse, A. Lantreibecq, R. Cours, M. Legros, H. Bensalah, J. Barjon, V. Mille, O. Brinza, J. Achard, Identification of dislocations in synthetic Chemically Vapor Deposited diamond single crystals, *Cryst. Growth Des.* 16 (2016) 2741–2746. <https://doi.org/10.1021/acs.cgd.6b00053>.
- [25] N. Davies, R. Khan, Martineau Philip, Gaukroger Mike, Twitchen Daniel, Harpreet Dhillon, Effect of off-axis growth on dislocations in CVD diamond grown on {001} substrates, *J. Phys. Conf. Ser.* 281 (2011) 012026.
- [26] A. Tallaire, M. Lesik, V. Jacques, S. Pezzagna, V. Mille, O. Brinza, J. Meijer, B. Abel, J.F. Roch, A. Gicquel, J. Achard, Temperature dependent creation of nitrogen-vacancy centers in single crystal CVD diamond layers, *Diam. Relat. Mater.* 51 (2015) 55–60.
- [27] N.B. Manson, M. Hedges, M.S.J. Barson, R. Ahlefeldt, M.W. Doherty, H. Abe, T. Ohshima, M.J. Sellars, NV⁻–N⁺ pair centre in 1b diamond, *New J. Phys.* 20 (2018) 113037. <https://doi.org/10.1088/1367-2630/aaec58>.

- [28] V. Stepanov, S. Takahashi, Determination of nitrogen spin concentration in diamond using double electron-electron resonance, *Phys. Rev. B.* 94 (2016) 024421.
<https://doi.org/10.1103/PhysRevB.94.024421>.
- [29] A.M. Edmonds, C.A. Hart, M.J. Turner, P.-O. Colard, J.M. Schloss, K. Olsson, R. Trubko, M.L. Markham, A. Rathmill, B. Horne-Smith, W. Lew, A. Manickam, S. Bruce, P.G. Kaup, J.C. Russo, M.J. DiMario, J.T. South, J.T. Hansen, D.J. Twitchen, R.L. Walsworth, Generation of nitrogen-vacancy ensembles in diamond for quantum sensors: Optimization and scalability of CVD processes, *ArXiv200401746 Cond-Mat Physicsquant-Ph.* (2020).
<http://arxiv.org/abs/2004.01746> (accessed April 12, 2020).
- [30] W. Wang, M. Hall, K. Moe, J. Tower, T. Moses, Latest-Generation CVD-Grown Synthetic Diamonds From Apollo Diamond Inc, *Gems Gemol.* 43 (2007) 294–312.
- [31] W. Wang, P. Doering, J. Tower, R. Lu, S. Eaton-Magaña, P. Johnson, E. Emerson, T.M. Moses, Strongly colored pink CVD lab-grown diamonds, *Gems Gemmol.* 46 (2010) 4–17.
- [32] A.M. Zaitsev, W. Wang, K.S. Moe, P. Johnson, Spectroscopic studies of yellow nitrogen-doped CVD diamonds, *Diam. Relat. Mater.* 68 (2016) 51–61.
<https://doi.org/10.1016/j.diamond.2016.06.002>.
- [33] A. Tallaire, A.T. Collins, D. Charles, J. Achard, R. Sussmann, A. Gicquel, M.E. Newton, A.M. Edmonds, R.J. Cruddace, Characterisation of high-quality thick single-crystal diamond grown by CVD with a low nitrogen addition, *Diam. Relat. Mater.* 15 (2006) 1700–1707.
<https://doi.org/10.1016/j.diamond.2006.02.005>.
- [34] R.U.A. Khan, P.M. Martineau, B.L. Cann, M.E. Newton, D.J. Twitchen, Charge transfer effects, thermo- and photochromism in single crystal CVD synthetic diamond, *J. Phys. Condens. Matter.* 21 (2009) 364214.
- [35] S. Liggins, Identification of point defects in treated single crystal diamond, PhD dissertation, Warwick, 2010. <http://webcat.warwick.ac.uk/record=b2491628~S15>.
- [36] A.M. Zaitsev, *Optical Properties of Diamond: A Data Handbook*, Springer-Verlag, Berlin Heidelberg, 2001. <https://doi.org/10.1007/978-3-662-04548-0>.

- [37] L.S. Hounscome, R. Jones, P.M. Martineau, D. Fisher, M.J. Shaw, P.R. Briddon, S. Öberg, Origin of brown coloration in diamond, *Phys. Rev. B.* 73 (2006) 125203.
- [38] A.M. Zaitsev, N.M. Kazuchits, V.N. Kazuchits, K.S. Moe, M.S. Rusetsky, O.V. Korolik, K. Kitajima, J.E. Butler, W. Wang, Nitrogen-doped CVD diamond: Nitrogen concentration, color and internal stress, *Diam. Relat. Mater.* 105 (2020) 107794.
<https://doi.org/10.1016/j.diamond.2020.107794>.
- [39] M.W. Dale, Colour centres on demand in diamond, PhD dissertation, Warwick, 2015.
<http://wrap.warwick.ac.uk/80044>.
- [40] B. Campbell, A. Mainwood, Radiation Damage of Diamond by Electron and Gamma Irradiation, *Phys. Status Solidi A.* 181 (2000) 99–107. [https://doi.org/10.1002/1521-396X\(200009\)181:1<99::AID-PSSA99>3.0.CO;2-5](https://doi.org/10.1002/1521-396X(200009)181:1<99::AID-PSSA99>3.0.CO;2-5).
- [41] M. De Feudis, A. Tallaire, L. Nicolas, O. Brinza, P. Goldner, G. Hétet, F. Bénédict, J. Achard, Large-Scale Fabrication of Highly Emissive Nanodiamonds by Chemical Vapor Deposition with Controlled Doping by SiV and GeV Centers from a Solid Source, *Adv. Mater. Interfaces.* n/a (2019) 1901408. <https://doi.org/10.1002/admi.201901408>.
- [42] M. Lesik, N. Raatz, A. Tallaire, P. Spinicelli, R. John, J. Achard, A. Gicquel, V. Jacques, J.-F. Roch, J. Meijer, S. Pezzagna, Production of bulk NV centre arrays by shallow implantation and diamond CVD overgrowth, *Phys. Status Solidi A.* 213 (2016) 2788–2788.
<https://doi.org/10.1002/pssa.201670666>.
- [43] G. Davies, Current problems in diamond: towards a quantitative understanding, *Phys. B Condens. Matter.* 273–274 (1999) 15–23. [https://doi.org/10.1016/S0921-4526\(99\)00398-1](https://doi.org/10.1016/S0921-4526(99)00398-1).
- [44] R. Giri, F. Gorrini, C. Dorigoni, C.E. Avalos, M. Cazzanelli, S. Tambalo, A. Bifone, Coupled charge and spin dynamics in high-density ensembles of nitrogen-vacancy centers in diamond, *Phys. Rev. B.* 98 (2018) 045401. <https://doi.org/10.1103/PhysRevB.98.045401>.
- [45] A. Jarmola, V.M. Acosta, K. Jensen, S. Chemerisov, D. Budker, Temperature- and Magnetic-Field-Dependent Longitudinal Spin Relaxation in Nitrogen-Vacancy Ensembles in Diamond, *Phys. Rev. Lett.* 108 (2012) 197601.

- [46] J. Choi, S. Choi, G. Kucsko, P.C. Maurer, B.J. Shields, H. Sumiya, S. Onoda, J. Isoya, E. Demler, F. Jelezko, N.Y. Yao, M.D. Lukin, Depolarization Dynamics in a Strongly Interacting Solid-State Spin Ensemble, *Phys. Rev. Lett.* 118 (2017) 093601.
<https://doi.org/10.1103/PhysRevLett.118.093601>.
- [47] A. Dréau, M. Lesik, L. Rondin, P. Spinicelli, O. Arcizet, J.F. Roch, V. Jacques, Avoiding power broadening in optically detected magnetic resonance of single NV defects for enhanced dc magnetic field sensitivity, *Phys. Rev. B.* 84 (2011) 195204.
- [48] J.F. Barry, J.M. Schloss, E. Bauch, M.J. Turner, C.A. Hart, L.M. Pham, R.L. Walsworth, Sensitivity optimization for NV-diamond magnetometry, *Rev. Mod. Phys.* 92 (2020) 015004.
<https://doi.org/10.1103/RevModPhys.92.015004>.